

**Analytic solutions of ultrahigh energy cosmic ray nuclei revisited**Markus Ahlers<sup>1</sup> and Andrew M. Taylor<sup>2</sup><sup>1</sup>*C.N. Yang Institute for Theoretical Physics, SUNY at Stony Brook, Stony Brook, New York 11794-3840, USA*<sup>2</sup>*ISDC, Chemin d'Ecogia 16, Versoix, CH-1290, Switzerland*

(Received 20 October 2010; published 20 December 2010)

The chemical composition of ultrahigh energy cosmic rays is a key question in particle astrophysics. The measured composition, inferred from the elongation rates of cosmic ray showers, looks in general very different from the initial source composition: resonant photo-disintegration in the cosmic radiation background proceeds rapidly at the highest energies and the initial composition quickly becomes lighter during propagation. For a statistical analysis of continuously improving cosmic ray data it is desirable to know the secondary spectra as precisely as possible. Here, we discuss exact analytic solutions of the evolution equation of ultrahigh energy cosmic ray nuclei. We introduce a diagrammatic formalism that leads to a systematic analytic expansion of the exact solution in terms of second order effects of the propagation. We show how the first order corrections of this expansion can improve the predictions of secondary spectra in a semianalytical treatment.

DOI: [10.1103/PhysRevD.82.123005](https://doi.org/10.1103/PhysRevD.82.123005)

PACS numbers: 96.50.S-, 13.85.Tp, 98.70.Sa

**I. INTRODUCTION**

The mass composition of ultrahigh energy (UHE) cosmic rays (CRs) remains an open question in astrophysics. The average mass number  $\langle A \rangle$  per energy can be inferred *directly* in CR observatories by the measurement of the elongation rate distribution of CR showers [1]. Presently, the observational situation is ambiguous despite strong experimental efforts over the years. Recent findings of the Pierre Auger Collaboration [2] indicate a transition of UHE CRs within the energy range  $10^{18}$  eV to  $4 \times 10^{19}$  eV from a light (presumably proton-dominated) spectrum towards a heavier composition [3]. In contrast, the HiRes Collaboration [4] finds a mass composition compatible with that of a proton-dominated spectrum [5].

Various features in the CR spectrum can also provide *indirect* evidence for the origin and composition of UHE CRs. The *ankle*—a hardening of the spectrum at  $3 \times 10^{18}$  eV—could be formed naturally by the superposition of two power-law fluxes and serves as a candidate of the transition between galactic and extragalactic cosmic rays [6,7]. It has also been advocated that this feature could be well reproduced by a proton-dominated power-law spectrum, where the ankle is formed as a *dip* in the spectrum from the energy loss of protons via Bethe-Heitler pair production [8,9]. In this case extragalactic protons could already start to dominate the spectrum beyond the *2nd knee* which corresponds to a slight *softening* of the spectrum at  $5 \times 10^{17}$  eV.

Proton dominance beyond the ankle is ultimately limited by the *Greisen-Zatsepin-Kuzmin* cutoff [10,11] due to resonant photo-pion production in the cosmic radiation background (CRB). In fact, a suppression of the CR spectrum at the expected energy of about  $5 \times 10^{19}$  eV has been detected by the Pierre Auger and HiRes collaborations at

a statistically significant level [4,12] and is consistent with a proton dominance at these energies. However, this feature could also originate from photo-disintegration of UHE CR nuclei in the cosmic background radiation, or from an *in situ* energy cutoff of the injection spectrum of UHE CR. To summarize, the interpretation of these experimental findings is as yet inconclusive and even controversial.

Simple theoretical arguments, however, can motivate a significant contribution of primary nuclei at energies beyond  $10^{18}$  eV. For the efficient acceleration of primary CRs to these extreme energies a particle should be confined magnetically in a suitable astrophysical environment. Since the particle's Larmor radius is proportional to its rigidity, i.e. its energy per charge, we expect that the maximal energy  $E_{\max}$  of UHE CRs to scale with the charge number  $Z$  of a (fully ionized) nucleus. The acceleration of heavy nuclei like iron ( $Z = 26$ ) can hence proceed up to larger energies and alleviates the fundamental limitations of cosmic accelerators to account for the observed spectrum of UHE CRs [13].

Analytic<sup>1</sup> descriptions of UHE CR propagation provide an easily accessible means of exploring both proton and heavy nuclei source scenarios. With the most recent results of the Auger collaboration indicating that the composition continues to become heavier at energies above  $3 \times 10^{19}$  eV, the heavy UHE CR flux component may well arrive from very local cosmological regions. To facilitate the future exploration of nearby UHE CR nuclei source distributions, we here develop further the analytic description of UHE CR nuclei propagation put forward in

<sup>1</sup>We use the term “analytic” here to denote *explicit* analytic solutions in closed form following [14]. There also exist many *implicit* analytic solutions for the spectra of UHE CRs that require an algorithmic treatment, e.g. [8,15,16].

Ref. [14]. These developments take into account subdominant energy losses, ensuring that this description provides an accurate means of obtaining the UHE CR flux over the full energy range covered by the cosmic ray observatories.

Numerical evaluations of the UHE CR spectra are equally viable, but can become time consuming since the evolution has to be traced over cosmologically scales of  $\mathcal{O}(\text{Gpc})$  whereas the interaction length of nuclei is of  $\mathcal{O}(\text{Mpc})$  at the highest energies. Our analytic treatment, instead, provides exact results up to propagation scales of  $\mathcal{O}(100 \text{ Mpc})$ , before the cosmic evolution of the radiation background and the source emission rates become relevant. The full propagation over cosmic distances can then be treated *semi-analytically* by multiple application of the analytic solution. Note, that the required evolution steps are much larger than in the case of a purely numerical solution with interaction lengths of  $\mathcal{O}(\text{Mpc})$ . Hence, the analytic approach does not only provide an alternative method for the evaluation and cross-check of CR spectra, but can also provide the basis of a more efficient numerical evaluation.

We will start in Sec. II with a short recapitulation of the compact evolution equations of UHE CR nuclei in the limit of a spatially homogeneous distribution of isotropic CR sources. We derive an exact analytic solution in Sec. III that includes continuous energy losses and multinucleon loss transitions between nuclei. In Sec. IV we introduce a perturbative expansions of the exact analytic solution that provides a convenient practical framework for next-to-leading order corrections of the solution given in Ref. [14]. We finally conclude in Sec. V.

## II. PROPAGATION OF COSMIC RAY NUCLEI

For a spatially homogeneous distribution of cosmic sources, emitting UHE particles of type  $i$ , the comoving number density  $Y_i$  is governed by a set of (Boltzmann) continuity equations of the form:

$$\begin{aligned} \dot{Y}_i &= \partial_E(HEY_i) + \partial_E(b_i Y_i) - \Gamma_i^{\text{tot}} Y_i \\ &+ \sum_j \int dE_j \gamma_{ji} Y_j + \mathcal{L}_i, \end{aligned} \quad (1)$$

together with the Friedman-Lemaître equations describing the cosmic expansion rate  $H(z)$  as a function of redshift  $z$ .<sup>2</sup> The first and second terms on the right-hand side describe, respectively, redshift and other continuous energy losses (CEL) with rate  $b \equiv dE/dt$ . The third and fourth terms

<sup>2</sup>This is given by  $H^2(z) = H_0^2[\Omega_m(1+z)^3 + \Omega_\Lambda]$ , normalized to its value today of  $H_0 \sim 70 \text{ km s}^{-1} \text{ Mpc}^{-1}$ , in the usual “concordance model” dominated by a cosmological constant with  $\Omega_\Lambda \sim 0.7$  and a (cold) matter component,  $\Omega_m \sim 0.3$  [13]. The time dependence of the redshift can be expressed via  $dz = -dt(1+z)H$ .

describe more general interactions involving particle losses ( $i \rightarrow \text{anything}$ ) with total interaction rate  $\Gamma_i^{\text{tot}}$ , and particle generation of the form  $j \rightarrow i$  with differential interaction rate  $\gamma_{ij}$ . The last term on the right-hand side,  $\mathcal{L}_i$ , corresponds to the emission rate of CRs of type  $i$  per comoving volume.

The two main reactions of UHE CR nuclei during their cosmic evolution are photo-disintegration [17–20] and Bethe-Heitler pair production [21] with the CRB. In addition to the dominant contribution of the cosmic microwave background (CMB) we also include the cosmic infrared/optical background (CIB) from Ref. [22] in our calculation of interaction and energy loss rates. Photo disintegration is dominated by the giant dipole resonance (GDR) with main branches  $A \rightarrow (A-1) + N$  and  $A \rightarrow (A-2) + 2N$  where  $N$  indicates a proton or neutron [17–19]. The GDR peak in the rest frame of the nucleus lies at about 20 MeV for one-nucleon emission, corresponding to  $E_{\text{GDR}}^A \simeq A \times 2 \times \epsilon_{\text{meV}}^{-1} \times 10^{10} \text{ GeV}$  in the cosmic frame with photon energies  $\epsilon = \epsilon_{\text{meV}} \text{ meV}$ . At energies below 10 MeV there exist typically a number of discrete excitation levels that can become significant for low mass nuclei. Above 30 MeV, where the photon wavelength becomes comparable or smaller than the size of the nucleus, the photon interacts via substructures of the nucleus. Out of these the interaction with quasideuterons is typically most dominant and forms a plateau of the cross section up to the photo-pion production threshold at  $\sim 145 \text{ MeV}$ . Bethe-Heitler pair production can be treated as a continuous energy loss process with rate  $b_A(z, E) = Z^2 b_p(z, E/A)$ , where  $b_p$  is the energy loss rate of protons [21]. The (differential) photo-disintegration rate  $\Gamma_{A \rightarrow B}(E)$  ( $\gamma_{A \rightarrow B}(E, E')$ ) is discussed in more detail in Appendix A.

The evolution of the spectra proceeds very rapidly on cosmic time scales and the flux of secondary nuclei,  $J$ , looks generally quite different from the initial injection spectrum,  $J_{\text{inj}}$ . The reaction network of nuclei depend in general on a large number of stable or long-lived isotopes. If the lifetime of an isotope is much shorter than its photo-disintegration rate it can be effectively replaced by its long-lived decay products in the network (1). Typically, neutron-rich isotopes  $\beta$  decay to a stable or long-lived nucleus with the same mass number. In most cases there is only one stable nucleus per mass number below  $^{56}\text{Fe}$  with the exception of the pairs  $^{54}\text{Cr}/^{54}\text{Fe}$ ,  $^{46}\text{Ca}/^{46}\text{Ti}$ ,  $^{40}\text{Ar}/^{40}\text{Ca}$  and  $^{36}\text{S}/^{36}\text{Ar}$ . We follow here the approach of *Puget, Stecker, and Bredekamp* (PSB) [18] and consider only a single nucleus per mass number  $A$  in the decay chain of primary iron  $^{56}\text{Fe}$ . This PSB chain of nuclei linked by one-nucleon losses is discussed in more detail in Appendix A.

As described earlier, CR nuclei that undergo rapid photo disintegration with CMB and CIB photons, carry a Lorentz factor of about  $\gamma = 2 \times 10^{10}$ . We can only strictly neglect long-lived secondary isotopes from the reaction network if

the nucleus lifetime in the cosmic frame,  $\gamma\tau$ , is much smaller than the inverse photo-disintegration rate, which is of the order of  $(4/A)$  Mpc. This corresponds to nucleon lifetimes of less than a few minutes. In general, there is a large number of isotopes below  $^{56}\text{Fe}$  that are sufficiently long-lived in the cosmic frame to take part in the photo-disintegration process (see Appendix A). Fortunately, a large degeneracy of intermediate isotopes with equal mass number affects only very heavy nuclei. The photo-disintegration of these degenerate nuclei, dominated by collective excitations of nucleons like the GDR, mostly depend on the mass number  $A$ . The fluxes calculated for nuclei in the PSB chain are expected to give a good representation of the total flux per mass number. Note that most of the analytic formulae that we are going to introduce in the following can be easily generalized to the case of the full reaction network including all isotopes.

Note, that the Boltzmann equations. (1) do not take into account the deflection of charged CR nuclei during their propagation through intergalactic and galactic magnetic fields. The strength of intergalactic magnetic fields is limited to the range  $10^{-16}$  G –  $10^{-9}$  G [23,24] and suggested to be of  $\mathcal{O}(10^{-12})$  G by simulations of large-scale structure formation [25]. In fact, if synchrotron radiation during propagation is negligible and the source distribution is homogenous, Eq. (1) provides a good approximation of the spectral evolution *even* for CRs having small rigidity which suffer large deflections [26]. However, magnetic inhomogeneities on small scales will suppress the spectrum of CRs with Larmor radius  $\ell_L < \ell_d$  where  $\ell_d$  is the characteristic distance between sources. It has been shown that for particularly strong intergalactic magnetic fields of strength  $\sim 1$  nG and coherence length of  $\sim 1$  Mpc, the diffusive propagation of CR protons will start to affect the spectrum below about  $10^9$  GeV if  $\ell_d \sim 50$  Mpc [27]. Depending on the diffusion regime, this can suppress the proton flux at  $10^8$  GeV by a factor of 3 to 100. Because of the dependence  $\ell_L \propto 1/Z$  we expect that for heavy nuclei diffusive propagation can in principle remain important up to the ankle. The results of this paper are based on solutions of Eqs. (1) and assume that the contribution of intergalactic or galactic magnetic fields can be neglected for the calculation of the UHE CR spectrum.

### III. ANALYTIC SOLUTION

The secondary nuclei produced via photo disintegration carry approximately the same Lorentz factor as the initial nucleus and the differential interaction rate in Eqs. (1) can be approximated as  $\gamma_{A \rightarrow B}(E, E') \simeq \Gamma_{A \rightarrow B}(E) \delta(E' - (B/A)E)$ . It is hence convenient to express the energy of a nucleus with mass number  $A$  and redshift  $z$  as  $A(1+z)E$  where  $E$  denotes the energy *per nucleon*. Introducing the CR density per comoving volume and nucleon energy,  $N_{A,i} \equiv \Delta E_i(1+z)AY_A(z, (1+z)AE_i)$ , and corresponding

emission rates,  $Q_{A,i} \equiv A(1+z)\Delta E_i \mathcal{L}(z, A(1+z)E_i)$  we can rewrite Eqs. (1) in the compact form<sup>3</sup>

$$\begin{aligned} \dot{N}_{A,i} \simeq & \Gamma_{A,i+1}^{\text{CEL}} N_{A,i+1} - \Gamma_{A,i}^{\text{CEL}} N_{A,i} - \sum_{B < A} \Gamma_{(A,i) \rightarrow (B,i)} N_{A,i} \\ & + \sum_{B > A} \Gamma_{(B,i) \rightarrow (A,i)} N_{B,i} + Q_{A,i}, \end{aligned} \quad (2)$$

where we define the rates

$$\begin{aligned} \Gamma_{A,i}^{\text{CEL}} &= \Gamma_{(A,i) \rightarrow (A,i-1)} \equiv \frac{b_A(z, A(1+z)E_i)}{A(1+z)\Delta E_i}, \\ \Gamma_{(A,i) \rightarrow (B,i)} &\equiv \Gamma_{A \rightarrow B}(z, A(1+z)E_i). \end{aligned} \quad (3)$$

Hooper *et al.* [14] discussed an analytical solution of Eqs. (2) for one-nucleon losses in the limit  $\Gamma_{A,i}^{\text{CEL}} = 0$  and  $Q_{A,i} = 0$ . In fact, the solution of a more general interaction network with generalized interaction rates  $\Gamma_{(A,i) \rightarrow (B,j)}$  of the form (3) can be written

$$\begin{aligned} N_{A,i}(t) = & \sum_{j \geq i, B \geq A} \sum_{\mathbf{c}} \left( \prod_{l=1}^{n_c-1} \Gamma_{c_l \rightarrow c_{l+1}} \right) \sum_{k=1}^{n_c} \left[ N_{B,j}(0) e^{-t \Gamma_{c_k}^{\text{tot}}} \right. \\ & \left. + \int_0^t dt' Q_{B,j}(t') e^{-(t-t') \Gamma_{c_k}^{\text{tot}}} \right] \prod_{p=1(\neq k)}^{n_c} \frac{1}{\Gamma_{c_p}^{\text{tot}} - \Gamma_{c_k}^{\text{tot}}}, \end{aligned} \quad (4)$$

where we sum over all possible production chains  $\mathbf{c} = \langle c_1, \dots, c_{n_c} \rangle$  with intermediate nuclei of mass number  $C$  in the energy bin  $k$ —denoted by the doublet  $c_i = (C, k)$ —and fixed end points  $c_1 = (B, j)$  and  $c_{n_c} = (A, i)$ . The partial width  $\Gamma_{c_l \rightarrow c_{l+1}}$  includes nucleon-disintegration ( $\Gamma_{(A,i) \rightarrow (B,i)}$ ) as well as CEL ( $\Gamma_{(A,i) \rightarrow (A,i-1)}$ ). Proof of Eq. (4) is given in Appendix A.

We can visualize the production chains  $\mathbf{c}$  diagrammatically as *paths* along the configuration grid of nuclei, as shown in Fig. 1. A horizontal link corresponds to a CEL transition whereas a vertical link denotes photo disintegration. The color coding in Fig. 1 indicates the type of the transition  $c_l \rightarrow c_{l+1}$ —green for CEL, red for one-nucleon losses and red-dotted for two-nucleon losses.<sup>4</sup> It is convenient to use this graphical representation as a shorthand notation for the terms of Eq. (4). To see this, we can write Eq. (4) in the form

$$\begin{aligned} N_{A,i}(t) = & \int_0^\infty dt' \sum_{j \geq i, B \geq A} G(A, i, B, j; t - t') [Q_{B,j}(t') \\ & + \delta(t') N_{B,j}(0)], \end{aligned} \quad (5)$$

<sup>3</sup>This form of the differential equation holds for nuclei heavier than beryllium. We can easily compensate for the process  $^9\text{Be} \rightarrow ^4\text{He} + ^4\text{He} + n$  of the PSB chain (see Appendix A) by redefining  $N'_{A,i} = N_{A,i}/2$  for  $A = 2, 3, 4$  and  $N'_{A,i} = N_{A,i}$  for other nuclei.

<sup>4</sup>We will use later on “generalized” chains, where the transition  $c_l \rightarrow c_{l+1}$  is not necessarily equal to  $\Gamma_{c_l \rightarrow c_{l+1}}$ .

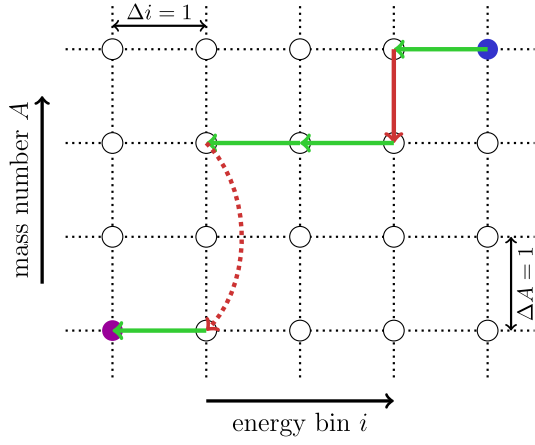


FIG. 1 (color online). A possible transition chain  $\mathbf{c}$  between an initial configuration (blue dot) and a final configuration (magenta dot) including one-nucleon losses (red arrows), two-nucleon losses (red-dotted arrows) and continuous energy loss (green arrows). For the exact analytic solution (4) all possible transition chains of this type are taken into account.

where we define a Green's function  $G(A, i, B, j; \Delta t) = \Theta(\Delta t) \sum_{\mathbf{c}} G(\mathbf{c}; \Delta t)$  as a sum over the contribution *per path*,

$$G(\mathbf{c}; \Delta t) \equiv \left( \prod_{l=1}^{n_{\mathbf{c}}-1} \Gamma_{c_l \rightarrow c_{l+1}} \right) \sum_{k=1}^{n_{\mathbf{c}}} e^{-\Delta t \Gamma_{c_k}^{\text{tot}}} \prod_{p=1 (\neq k)}^{n_{\mathbf{c}}} \frac{1}{\Gamma_{c_p}^{\text{tot}} - \Gamma_{c_k}^{\text{tot}}}. \quad (6)$$

Each term  $G(\mathbf{c}; \Delta t)$  in the previous equation corresponds to a production chain on the configuration grid. We will use this graphical representation later for a perturbative expansions of Eq. (4).

The interaction rates  $\Gamma_A$  and energy loss rates  $b_A$  are not constant as the Universe expands. The adiabatic expansion of the CMB number density (see Appendix A) results in a redshift dependence of interaction rates and energy loss rates as  $\Gamma_A(z, E) = (1+z)^3 \Gamma_A(0, (1+z)E)$  and  $b_A(z, E) = (1+z)^2 b_A(0, (1+z)E)$ , respectively. The redshift scaling of the CIB [22] is less trivial since it follows the star formation rate. For the corresponding redshift dependence of the rates we refer to the discussion of Ref. [16]. Also, the nucleus emission rates  $\mathcal{L}_A$  are not in general constant with time. A standard approach approximates the scaling with redshift as a simple power law over a finite redshift distance, e.g.

$$\mathcal{L}_A(z, E) \equiv \Theta(z - z_{\min}) \Theta(z_{\max} - z) (1+z)^n \mathcal{L}_A(0, E). \quad (7)$$

We can account for the redshift dependence of  $\Gamma$  and  $Q$  by summing Eqs. (4) over sufficiently small redshift intervals, in which these quantities can be regarded as constant. Typically, intervals of  $\Delta z \approx 0.01$  are sufficient for this approach.

Though the expression (4) is an *exact* analytical solution of the system of differential Eqs. (2), its calculation

involves a large number of possible production chains and becomes numerically inefficient for large configuration grids.<sup>5</sup> For instance, for one-nucleon *and* two-nucleon losses the number of possible chains  $F_{\Delta A}$  between nuclei with mass number  $A$  and  $B = A + \Delta A$  can be derived iteratively from the identity  $F_{\Delta A+2} = F_{\Delta A} + F_{\Delta A+1}$  with  $F_0 = F_1 = 1$ , which we recognize as the sequence of *Fibonacci* numbers. Hence, the total sum over different chains and  $N$  primary nuclei in expression (4) involves  $F_0 + F_1 + \dots + F_{N-1} = F_{N+1} - 1$  number of terms, which is a number that scales exponentially with  $N$ . Hence, considering all transitions via one-nucleon and two-nucleon losses between, say, proton ( $A = 1$ ) and iron ( $A = 56$ ) becomes numerically very expensive even without considering transitions via CEL.

We show in the following that the exact expression (4) can be well approximated by the dominant production chain through one-nucleon losses. Corrections via two-nucleon losses and CEL can be treated perturbatively. As means of a comparative check, we obtain results using our analytic description, assuming a source injection spectrum of the form

$$J_{\text{inj}} \propto E^{-\gamma} e^{-E/E_{\text{max}}}. \quad (8)$$

These analytic results are compared against those obtained numerically through a Runge-Kutta method [30].

## IV. PERTURBATIVE APPROACH

The dominant contribution to the nucleon transitions in the CRB comes from one-nucleon losses with transition rate  $\Gamma_{A,i}^{\text{1N}}$ . In the following we focus on perturbative corrections to this dominant decay route from the contributions of two-nucleon losses and CEL with transition rates  $\Gamma_{A,i}^{\text{2N}}$  and  $\Gamma_{A,i}^{\text{CEL}}$ , respectively.

### A. Two-Nucleon losses

We start with perturbative corrections from two-nucleon losses and assume, for the moment, that  $\Gamma_{A,i}^{\text{tot}} = \Gamma_{A,i}^{\text{1N}} + \Gamma_{A,i}^{\text{2N}}$  and  $\Gamma_{A,i}^{\text{CEL}} = 0$ . For a perturbative expansion it is convenient to rewrite Eq. (B2) as

$$N_{A,i}(t) = \sum_{B \geq A} \sum_{C=A}^B \mathcal{F}_{ABC}^i \left( \prod_{D=A+1}^B \Gamma_{D,i}^{\text{tot}} \right) \left[ N_{B,i}(0) e^{-t \Gamma_{C,i}^{\text{tot}}} + \int_0^t dt' Q_{B,i}(t') e^{-(t-t') \Gamma_{C,i}^{\text{tot}}} \right] \prod_{D=A(\neq C)}^B \frac{1}{\Gamma_{D,i}^{\text{tot}} - \Gamma_{C,i}^{\text{tot}}}, \quad (9)$$

<sup>5</sup>In general, the numerical evaluation of expression (4) requires a high computational precision. We use the publicly available multiple precision libraries GMP [28] and MPFR [29] for this purpose.

with

$$\mathcal{F}_{ABC}^i \equiv \sum_{\mathbf{c}} \left( \prod_{l=1}^{n_{\mathbf{c}}-1} \frac{\Gamma_{c_l \rightarrow c_{l+1}}}{\Gamma_{c_l}^{\text{tot}}} \right) \prod_{D=A+1}^B \left( 1 - \frac{\Gamma_{C,i}^{\text{tot}}}{\Gamma_{D,i}^{\text{tot}}} \right). \quad (10)$$

We can define a perturbative expansion of Eq. (10) in terms of subdominant branching ratios of two-nucleon production,  $\Gamma_{C,i}^{2N}/\Gamma_{C,i}^{\text{tot}}$ . The leading order (LO) contribution,  $\mathcal{F}_{ABC}^{i,\text{LO}} = 1$ , reproduces the approximation of Ref. [14]. The next-to-leading order (NLO) contribution can be written as

$$\mathcal{F}_{ABC}^{i,\text{NLO}} = \sum_{D=A+2}^B \frac{\Gamma_{D,i}^{2N}}{\Gamma_{D,i}^{\text{tot}}} \left( 1 - \frac{\Gamma_{C,i}^{\text{tot}}}{\Gamma_{D-1,i}^{\text{tot}}} \right) - \sum_{D=A+1}^B \frac{\Gamma_{D,i}^{2N}}{\Gamma_{D,i}^{\text{tot}}}. \quad (11)$$

We can most easily visualize these terms by a perturbative expansion of the nucleon densities,

$$N_{A,i} = \sum_{n \geq 0} N_{A,i}^{(n)}, \quad (12)$$

where the terms  $N_{A,i}^{(n)}$  are solutions to the set of differential equations,

$$\begin{aligned} \dot{N}_{A,i}^{(0)} &= -\Gamma_{A,i}^{\text{tot}} N_{A,i}^{(0)} + \Gamma_{A+1,i}^{\text{tot}} N_{A+1,i}^{(0)} + Q_{A,i}, \\ \dot{N}_{A,i}^{(n)} &= -\Gamma_{A,i}^{\text{tot}} N_{A,i}^{(n)} + \Gamma_{A+1,i}^{\text{tot}} N_{A+1,i}^{(n)} + \Gamma_{A+2,i}^{2N} N_{A+2,i}^{(n-1)} \\ &\quad - \Gamma_{A+1,i}^{2N} N_{A+1,i}^{(n-1)}, \quad (n > 0). \end{aligned} \quad (13)$$

For the moment, we assume that the total width  $\Gamma_{A,i}^{\text{tot}}$  is the sum of one-nucleon and two-nucleon losses. This, however, can be generalized to the total photo-disintegration rate for general nucleon losses (see Sec. IV B). As an initial condition we define  $N_{A,i}^{(n)}(0) = 0$  for  $n > 0$  and  $N_{A,i}^{(0)}(0) = N_{A,i}(0)$ . Note, that with this initial condition the expansion (12) becomes finite and hence converges trivially. Each term  $N^{(n)}$  corresponds, by construction, to the  $n$ -th order correction of  $\mathcal{F}$ . We can write the NLO correction explicitly as

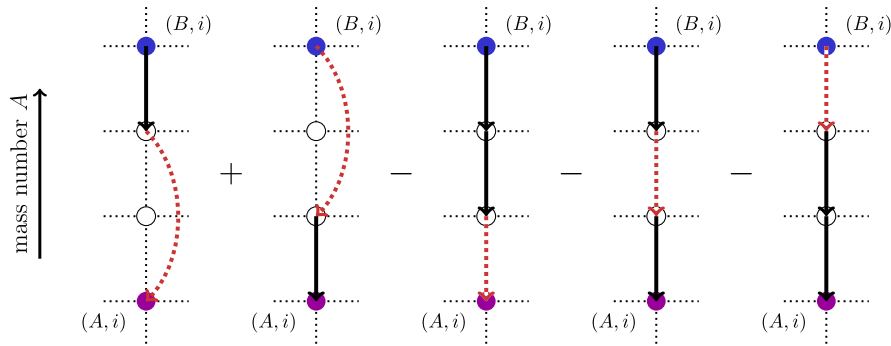


FIG. 2 (color online). A graphic representation of the NLO paths contributing in the first correction  $N_{A,i}^{(1)}$  for  $\Delta A = 3$  [see Eq. (14)]. The black arrows indicate transitions between configurations with total transition rate  $\Gamma_{A,i}^{\text{tot}} = \Gamma_{A,i}^{1N} + \Gamma_{A,i}^{2N}$  and the dotted red arrows two-nucleon transition rates  $\Gamma_{A,i}^{2N}$ , respectively. Note that these types of graphs contribute with *opposite* sign in Eq. (14).

$$\begin{aligned} N_{A,i}^{(1)}(t) &= \sum_{B \geq A} \sum_{C=A}^B \left( \prod_{D=A+1}^B \Gamma_{D,i}^{\text{tot}} \right) \left[ \int_0^t dt' (\Gamma_{B+2,i}^{2N} N_{B+2,i}^{(0)}(t') \right. \\ &\quad \left. - \Gamma_{B+1,i}^{2N} N_{B+1,i}^{(0)}(t') \right) e^{-(t-t')\Gamma_{C,i}^{\text{tot}}} \prod_{D=A(\neq C)}^B \frac{1}{\Gamma_{D,i}^{\text{tot}} - \Gamma_{C,i}^{\text{tot}}}. \end{aligned} \quad (14)$$

Inserting the LO solution in Eq. (14) and following similar algebraic steps as in Appendix B one can identify  $N^{(1)}$  as the *difference* of contributions from paths  $\langle (A, i), \dots, (B, i) \rangle$  with length  $B - A + 1$  and  $B - A$ , respectively, with the *single* insertion of a two-nucleon loss step into the decay chain. This is displayed diagrammatically in Fig. 2 for the case  $\Delta A = 3$ .

Note, that we can also express Eqs. (14) as a matrix equation of the form,

$$N_{A,i}^{(1)}(\Delta t) \simeq \sum_{B \geq A} (\mathcal{X}_{AB,i}(\Delta t) N_{B,i}(0) + \mathcal{Y}_{AB,i}(\Delta t) Q_{B,i}). \quad (15)$$

The matrices  $\mathcal{X}(\Delta t)$  and  $\mathcal{Y}(\Delta t)$  are in general only slowly changing with the redshift scaling of the background radiation. It is hence possible to improve the NLO results by introducing sufficiently small time intervals  $\Delta z$  and apply Eq. (15) repeatedly.

We show the LO and NLO results of our approach in comparison to a numerical solution via a Runge-Kutta method in Fig. 3. For simplicity, we assume that CEL is absent and that source terms and interaction rates are constant throughout the integration domain  $0 < z < 1$ . The NLO contributions are shown for two cases. In the case “ $\Delta z = 1$ ” we calculate the NLO contribution directly by Eq. (14). The case “ $\Delta z = 0.01$ ” shows the improvement of the NLO contribution by a repeated application of Eq. (15) for the corresponding time interval—100 times in this case. In most cases, the LO approximation is already satisfactory [14].

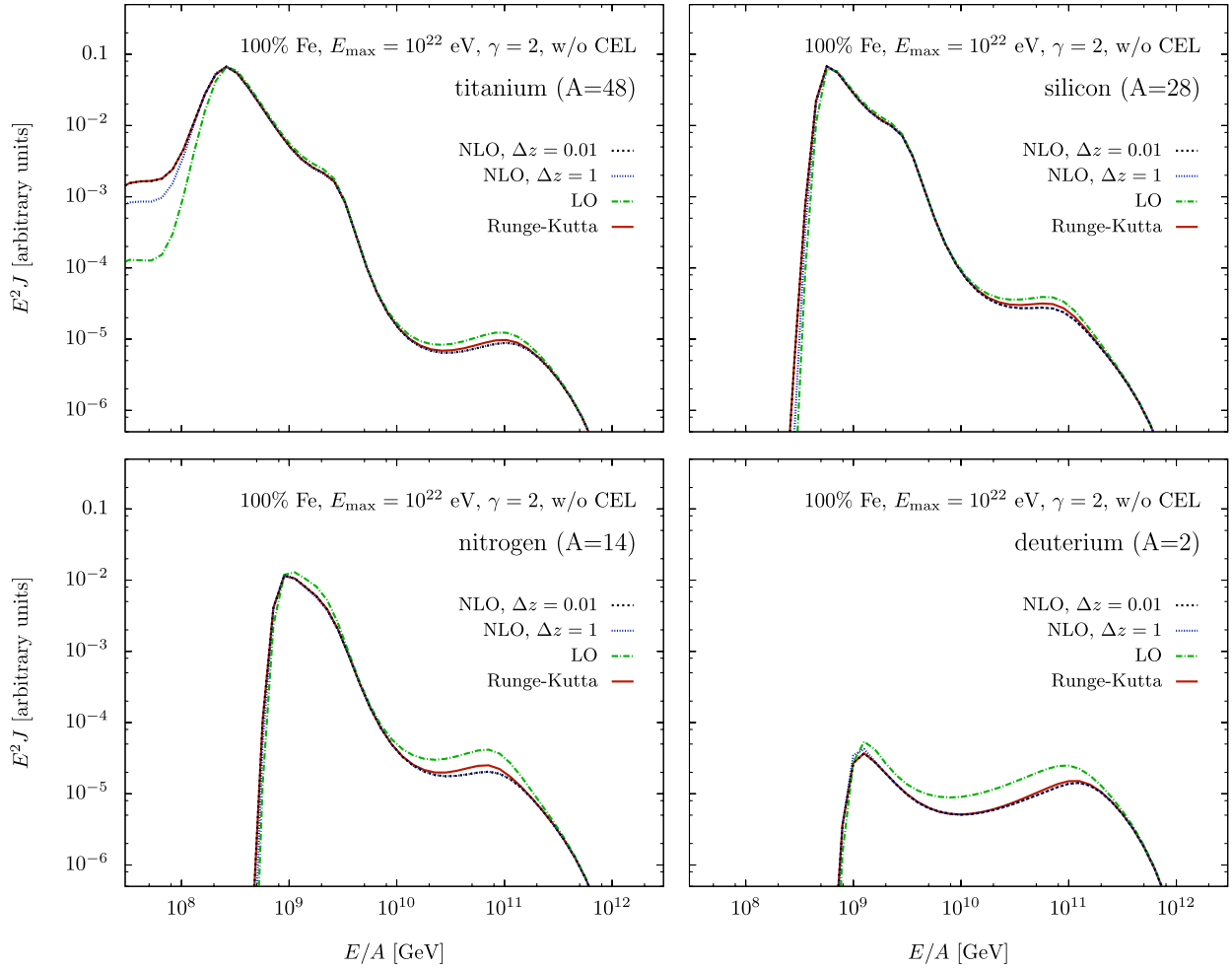


FIG. 3 (color online). The solution (9) at LO and up to NLO [Eq. (14)] for one-nucleon (1N) and two-nucleon (2N) losses. To aid the comparison between the results, we ignore the evolution of the nucleon emission rates and interaction rates with redshift and sum over redshift steps  $\Delta z = 0.01$ . We compare the LO and NLO analytic results to a numerical solution via a Runge-Kutta method [30].

### B. General photo-disintegration losses

For high mass nuclei ( $A \gtrsim 40$ ) of the PSB chain one-nucleon and two-nucleon losses constitute more than 90% of the total photo-disintegration rate as can be seen in the Table I. However, for low mass nuclei the emission of  $\alpha$  particles [as well as deuterons (D) and tritons (T)] can become important. As in the previous section, we can organize these subleading contributions via the expansion (12). For instance, the additional contribution from  $\alpha$  particle loss can be introduced at NLO ( $n > 0$ ) as

$$\begin{aligned} \dot{N}_{A,i}^{(n)} = & -\Gamma_{A,i}^{\text{tot}} N_{A,i}^{(n)} + \Gamma_{A+1,i}^{\text{tot}} N_{A+1,i}^{(n)} + \Gamma_{A+2,i}^{2N} N_{A+2,i}^{(n-1)} \\ & - \Gamma_{A+1,i}^{2N} N_{A+1,i}^{(n-1)} + \Gamma_{A+4,i}^{\alpha} N_{A+4,i}^{(n-2)} - \Gamma_{A+1,i}^{\alpha} N_{A+1,i}^{(n-2)}, \end{aligned} \quad (16)$$

where we now have to include  $\alpha$  emission in the definition of the total rate,  $\Gamma_{A,i}^{\text{tot}} = \Gamma_{A,i}^{1N} + \Gamma_{A,i}^{2N} + \Gamma_{A,i}^{\alpha}$ . The treatment of these additional photo-disintegration channels is completely analogous to the case of two-nucleon losses.

### C. Continuous energy losses

We next consider the contribution of CEL to the solution (4). In this case we have to include all possible paths in Eq. (4) that allow for both, variation of energy *and* mass number as the one shown in the left panel of Fig. 1. Similar to the discussion of two-nucleon losses, the number of possible paths becomes very large. For the remainder of this section we consider only one-nucleon photo-disintegration losses together with CEL and, hence,  $\Gamma_{A,i}^{\text{tot}} = \Gamma_{A,i}^{1N} + \Gamma_{A,i}^{\text{CEL}}$ . Despite this simplification there are still  $(\Delta A + \Delta i)! / (\Delta A)! / (\Delta i)!$  different paths in total between the two configurations  $(A, i)$  and  $(A + \Delta A, i + \Delta i)$ . This becomes computationally very expensive for long production chains, as we already observed for the introduction of two-nucleon losses.

We can account for CEL transitions as effective source terms in the differential Eqs. (2). This turns out to be an efficient way for determining the resulting spectra. As before, we can use the perturbative expansion (12) of the

TABLE I. The nuclei of the *Puget-Stecker-Bredekamp* chain [18] and the relative contribution of inclusive channels to the total photo-disintegration cross section in the CMB and CIB calculated by TALYS [20]. We assume an  $E^{-2}$  spectrum of the nuclei and integrate over nucleon energies  $10^{17}\text{eV} < E/A < 10^{21}\text{eV}$ . Channels with contribution less than 1% are omitted in the table.

Nucleus	$(\gamma, n)$	$(\gamma, p)$	$(\gamma, np)$	$(\gamma, 2n)$	$(\gamma, 2p)$	$(\gamma, \alpha)$	$(\gamma, n\alpha)$	$(\gamma, p\alpha)$	$(\gamma, 2\alpha)$	$(\gamma, D)$	$(\gamma, T)$	$(\gamma, {}^3\text{He})$	Total
<sup>56</sup> Fe	0.74	0.12	0.02	0.05	...	0.02	...	...	...	...	...	...	0.95
<sup>55</sup> Mn	0.80	0.04	0.01	0.09	...	...	...	...	...	...	...	...	0.95
<sup>54</sup> Cr	0.74	0.01	0.01	0.18	...	0.01	...	...	...	...	...	...	0.95
<sup>53</sup> Cr	0.86	0.03	0.02	0.07	...	...	...	...	...	...	...	...	0.97
<sup>52</sup> Cr	0.74	0.11	0.01	0.07	...	0.02	...	...	...	...	...	...	0.96
<sup>51</sup> V	0.79	0.01	...	0.16	...	...	...	...	...	...	...	...	0.96
<sup>50</sup> Ti	0.79	0.01	...	0.16	...	...	...	...	...	...	...	...	0.96
<sup>49</sup> Ti	0.84	0.03	0.02	0.08	...	...	...	...	...	...	...	...	0.97
<sup>48</sup> Ti	0.74	0.11	0.02	0.07	...	0.02	...	...	...	...	...	...	0.95
<sup>47</sup> Ti	0.81	0.07	0.05	0.02	...	0.01	...	...	...	...	...	...	0.97
<sup>46</sup> Ti	0.35	0.46	0.03	0.02	0.03	0.06	...	...	...	...	...	...	0.96
<sup>45</sup> Sc	0.55	0.27	0.09	0.03	...	0.02	...	...	...	...	...	...	0.96
<sup>44</sup> Ca	0.73	0.04	0.01	0.15	...	0.02	...	...	...	...	...	...	0.95
<sup>43</sup> Ca	0.74	0.06	0.03	0.08	...	0.03	0.04	...	...	...	...	...	0.97
<sup>42</sup> Ca	0.37	0.29	0.03	0.07	0.01	0.19	0.01	...	...	...	...	...	0.96
<sup>41</sup> Ca	0.28	0.41	0.13	...	0.01	0.11	0.01	...	...	...	...	...	0.97
<sup>40</sup> Ca	0.02	0.66	0.02	...	0.17	0.09	...	0.01	...	...	...	...	0.97
<sup>39</sup> K	0.08	0.65	0.10	...	0.01	0.10	...	0.03	...	...	...	...	0.98
<sup>38</sup> Ar	0.46	0.21	0.04	0.05	0.01	0.17	0.01	...	...	...	...	...	0.94
<sup>37</sup> Cl	0.65	0.11	0.04	0.09	...	0.05	0.01	...	...	...	...	...	0.95
<sup>36</sup> S	0.68	0.01	0.01	0.23	...	0.02	0.01	...	...	...	...	...	0.96
<sup>35</sup> Cl	0.12	0.58	0.11	...	...	0.13	...	0.02	...	...	...	...	0.97
<sup>34</sup> S	0.60	0.13	0.03	0.08	...	0.09	0.01	...	...	...	...	...	0.95
<sup>33</sup> S	0.44	0.23	0.10	...	...	0.13	0.06	...	...	0.01	...	...	0.97
<sup>32</sup> S	0.05	0.63	0.04	...	0.10	0.14	...	0.01	...	...	...	...	0.97
<sup>31</sup> P	0.24	0.49	0.13	...	...	0.07	...	0.01	...	0.01	...	...	0.96
<sup>30</sup> Si	0.69	0.04	0.02	0.17	...	0.03	0.01	...	...	...	...	...	0.96
<sup>29</sup> Si	0.65	0.15	0.08	...	...	0.06	0.02	...	...	0.01	...	...	0.97
<sup>28</sup> Si	0.10	0.55	0.04	...	0.06	0.16	...	0.01	...	...	...	...	0.93
<sup>27</sup> Al	0.22	0.44	0.15	0.01	...	0.10	...	0.01	...	0.01	...	...	0.94
<sup>26</sup> Mg	0.68	0.04	0.01	0.17	...	0.03	0.01	...	...	...	...	...	0.95
<sup>25</sup> Mg	0.64	0.08	0.08	...	...	0.10	0.06	...	...	0.01	...	...	0.97
<sup>24</sup> Mg	0.08	0.53	0.03	...	0.03	0.25	...	...	0.02	...	...	...	0.96
<sup>23</sup> Na	0.27	0.40	0.10	0.01	...	0.15	0.01	...	0.02	0.01	...	...	0.96
<sup>22</sup> Ne	0.65	0.02	0.01	0.17	...	0.06	0.03	...	...	...	...	...	0.95
<sup>21</sup> Ne	0.49	0.05	0.04	...	...	0.21	0.16	...	0.01	0.01	...	...	0.96
<sup>20</sup> Ne	0.02	0.22	0.02	...	...	0.49	0.03	0.06	0.11	0.01	...	...	0.96
<sup>19</sup> F	0.27	0.12	0.07	0.01	...	0.35	0.08	0.01	...	0.01	0.01	...	0.93
<sup>18</sup> O	0.50	...	...	0.28	...	0.09	0.06	...	...	...	...	...	0.94
<sup>17</sup> O	0.46	...	0.05	0.01	...	0.24	0.19	...	...	0.01	...	...	0.97
<sup>16</sup> O	0.09	0.29	0.03	...	...	0.36	...	0.01	0.11	0.02	...	...	0.92
<sup>15</sup> N	0.38	0.10	0.15	0.02	...	0.22	...	...	...	0.02	0.02	...	0.92
<sup>14</sup> N	0.15	0.31	0.24	...	...	0.10	0.01	0.01	0.01	0.07	...	...	0.91
<sup>13</sup> C	0.51	0.01	0.03	0.01	...	0.29	0.13	...	...	...	...	...	0.97
<sup>12</sup> C	0.11	0.21	0.01	...	...	0.57	0.01	0.02	...	0.01	...	...	0.94
<sup>11</sup> B	0.21	0.05	0.04	0.01	...	0.32	0.10	...	...	0.05	0.11	...	0.89
<sup>10</sup> B	0.14	0.21	0.03	...	...	0.38	-	0.01	...	0.17	0.01	0.01	0.96

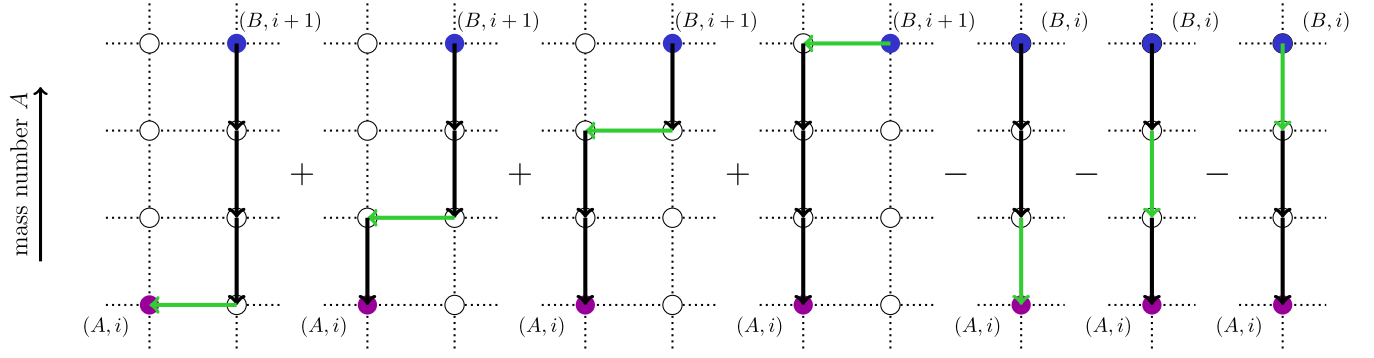


FIG. 4 (color online). A graphic representation of the NLO paths contributing in the first correction  $N_{A,i}^{(1)}$  for  $\Delta A = 3$  [see Eq. (18)]. The black arrows indicate transitions between configurations with total transition rate  $\Gamma_{A,i}^{\text{tot}} = \Gamma_{A,i}^{\text{IN}} + \Gamma_{A,i}^{\text{CEL}}$  and the green arrows transitions with CEL rate  $\Gamma_{A,i}^{\text{CEL}}$ , respectively. Note that these types of graphs contribute with *opposite* sign in Eq. (18).

nucleon densities, where the terms  $N_{A,i}^{(n)}$  are now solutions to the set of differential equations,

$$\begin{aligned} \dot{N}_{A,i}^{(0)} &= -\Gamma_{A,i}^{\text{tot}} N_{A,i}^{(0)} + \Gamma_{A+1,i}^{\text{tot}} N_{A+1,i}^{(0)} + Q_{A,i}, \\ \dot{N}_{A,i}^{(n)} &= -\Gamma_{A,i}^{\text{tot}} N_{A,i}^{(n)} + \Gamma_{A+1,i}^{\text{tot}} N_{A+1,i}^{(n)} + \Gamma_{A,i+1}^{\text{CEL}} N_{A,i+1}^{(n-1)} \\ &\quad - \Gamma_{A+1,i}^{\text{CEL}} N_{A+1,i}^{(n-1)}, \quad (n > 0). \end{aligned} \quad (17)$$

Here, the total width  $\Gamma_{A,i}^{\text{tot}} = \Gamma_{A,i}^{\text{IN}} + \Gamma_{A,i}^{\text{CEL}}$  is now for the sum of one-nucleon and CEL, though in general it would receive contributions from all exclusive channels. Note that with the initial condition  $N_{A,i}^{(n)}(0) = 0$  for  $n > 0$  the expansion (12) of  $N_{A,i}$  is finite if a finite set of energy bins and nuclei is considered,  $A \leq A_{\text{max}}$  and  $i \leq i_{\text{max}}$ . More specifically, the expansion of  $N_{A,i}$  only includes nonzero terms  $N_{A,i}^{(n)}$  for  $n \leq (A_{\text{max}} + i_{\text{max}}) - (A + i)$ .

The first term  $N_{A,i}^{(0)}$  in the expansion of  $N_{A,i}$  is our familiar solution for the one-nucleon loss case (9) where the partial width is replaced by the total width. The second term  $N^{(1)}$  can be evaluated explicitly by an insertion of  $N^{(0)}$ ,

$$\begin{aligned} N_{A,i}^{(1)}(t) &= \sum_{B \geq A} \sum_{C=A}^B \left( \prod_{D=A+1}^B \Gamma_{D,i}^{\text{tot}} \right) \left[ \int_0^t dt' (\Gamma_{B,i+1}^{\text{CEL}} N_{B,i+1}^{(0)}(t') \right. \\ &\quad \left. - \Gamma_{B+1,i}^{\text{CEL}} N_{B+1,i}^{(0)}(t') \right) e^{-(t-t')\Gamma_{C,i}^{\text{tot}}} \prod_{D=A(\neq C)}^B \frac{1}{\Gamma_{D,i}^{\text{tot}} - \Gamma_{C,i}^{\text{tot}}}. \end{aligned} \quad (18)$$

After some algebraic manipulations one can identify  $N^{(1)}$  as the *difference* of contributions from paths  $\langle (A, i), \dots, (B, i+1) \rangle$  and  $\langle (A, i), \dots, (B, i) \rangle$  with the *single* insertion of CEL step into the decay chain. This is indicated diagrammatically in Fig. 4 for the case  $\Delta A = 3$ .

Note that the NLO correction for CEL only introduces transitions between the energy bins  $i$  and  $i+1$ . Hence, the NLO solution (18) can not be considered as a small

correction to the full solution if the contribution from CEL becomes large,  $\Delta t \Gamma_{A,i}^{\text{CEL}} \gtrsim 1$ . However, in analogy to the case of two-nucleon losses we can write the NLO contribution as a matrix equation

$$\begin{aligned} N_{A,i}^{(1)}(\Delta t) &\simeq \sum_{B \geq A} (\mathcal{X}_{AB,i}(\Delta t) N_{B,i}(0) + \mathcal{Y}_{AB,i}(\Delta t) Q_{B,i} \\ &\quad + \mathcal{V}_{AB,i}(\Delta t) N_{B,i+1}(0) + \mathcal{W}_{AB,i}(\Delta t) Q_{B,i+1}). \end{aligned} \quad (19)$$

If we consider *sufficiently* small time intervals  $\Delta t$  such that  $\Delta t \Gamma_{A,i}^{\text{CEL}} \ll 1$  we can approximate the exact solution by a repeated application of Eq. (19). The transition matrices  $\mathcal{X}(\Delta t)$ ,  $\mathcal{Y}(\Delta t)$ ,  $\mathcal{V}(\Delta t)$  and  $\mathcal{W}(\Delta t)$  are only slowly changing with the scaling of the background radiation. It is hence only necessary to re-evaluate these matrices on large time-scales; typically  $\Delta z \simeq 0.01$  is sufficient for the propagation of heavy nuclei. Thus, results obtained by the application of this procedure should be considered *semi-analytic*.

Figure 5 shows the results of the LO and NLO energy flux spectra compared with results obtained using a Runge-Kutta method. For simplicity, we again consider constant source terms and interaction rates and assume that two-nucleon losses are absent. The repeated application of Eq. (19) reproduces the numerical solution well. For heavy nuclei (and hence “short” transitions from primary iron) or large energies  $E/A > 10^{10}$  GeV the LO contribution is already an excellent approximation. The full NLO correction including two-nucleon loss and redshift evolution of the sources and interaction rates is then shown in Fig. 6.

#### D. Secondary proton and helium spectra

Finally, we discuss an expansion of the spectrum of primary and secondary protons<sup>6</sup> and helium. This case is

<sup>6</sup>We do not distinguish between protons and neutrons in the following, assuming a prompt decay of secondary neutrons.



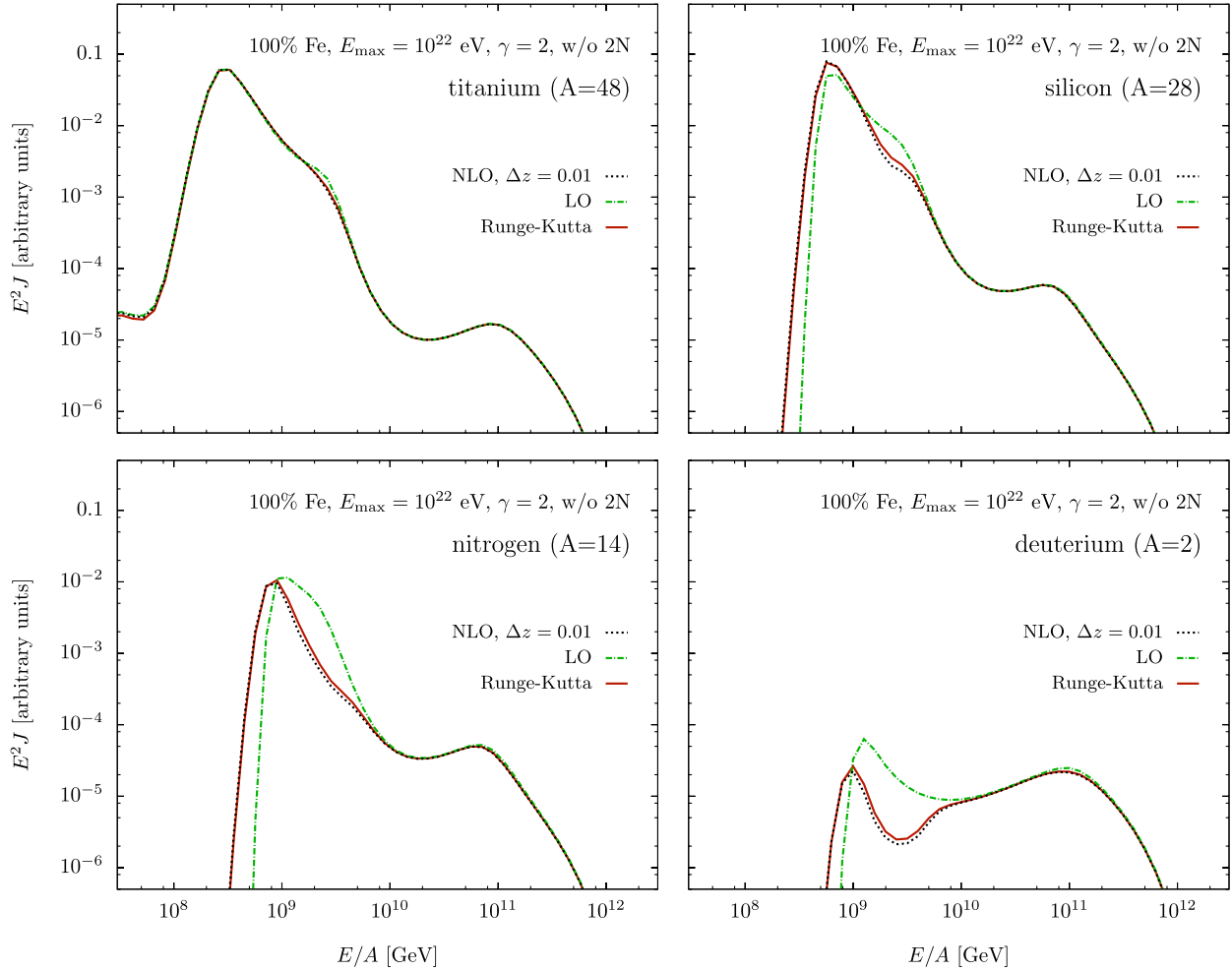


FIG. 5 (color online). Comparison of the terms in expression (9) up to NLO with the numerical solution via a Runge-Kutta method including one-nucleon (1N) and CEL. To aid the comparison between the results, we ignore the evolution of the nucleon emission rates and interaction rates with redshift and sum over redshift steps  $\Delta z = 0.01$ .

slightly different from the propagation of heavy nuclei, since there are additional contributions from the channels  $(\gamma, N)$ ,  $(\gamma, 2N)$ ,  $(\gamma, \alpha)$ ,  $(\gamma, N\alpha)$  and  $(\gamma, 2\alpha)$ . Secondary nucleon production follows the differential equation

$$\dot{N}_{1,i} \approx \Gamma_{1,i+1}^{\text{CEL}} N_{1,i+1} - \Gamma_{1,i}^{\text{CEL}} N_{1,i} + \sum_{A \geq 2} \Gamma_{A,i}^{\text{eff},N} N_{A,i} + Q_{1,i}, \quad (20)$$

where the effective nucleon production rate  $\Gamma_{A,i}^{\text{eff},N}$  from transitions  $(A, i) \rightarrow (1, i)$  is defined as

$$\Gamma_{A,i}^{\text{eff},N} \equiv \Gamma_{A,i}^{\text{1N}} + 2\Gamma_{A,i}^{\text{2N}} + \Gamma_{A,i}^{\text{N}\alpha} + \delta_{A2} \Gamma_{2,i}^{\text{1N}} + \delta_{A3} \Gamma_{3,i}^{\text{2N}} + \delta_{A6} \Gamma_{6,i}^{\text{N}\alpha}, \quad (21)$$

with  $\delta_{AB} = 1$  if  $A = B$  and zero otherwise.<sup>7</sup> Note, that the last term in (21) is assumed absent in the PSB chain. Photo-

hadronic interactions of the protons with the CMB and CIB can be determined using the Monte Carlo package SOPHIA [31]. Here, we approximate photo-pion interactions of the protons as a continuous energy loss process in addition to Bethe-Heitler pair production. The differential Eq. (20) is of the same form as Eq. (2) and we can hence write its exact solution in the form (4).

With the expansion (9) we can write the set of evolution equations as

$$\begin{aligned} \dot{N}_{1,i}^{(0)} &\approx -\Gamma_{1,i}^{\text{CEL}} N_{1,i}^{(0)} + \Gamma_{1,i+1}^{\text{CEL}} N_{1,i+1}^{(0)} + \sum_{A \geq 2} \Gamma_{A,i}^{\text{eff}} N_{A,i}^{(0)} + Q_{1,i}, \\ \dot{N}_{1,i}^{(n)} &\approx -\Gamma_{1,i}^{\text{CEL}} N_{1,i}^{(n)} + \Gamma_{1,i+1}^{\text{CEL}} N_{1,i+1}^{(n)} \\ &\quad + \sum_{A \geq 2} \Gamma_{A,i}^{\text{eff}} N_{A,i}^{(n)}, \quad (n > 0). \end{aligned} \quad (22)$$

In contrast to the case of nuclei, we cannot treat CEL of the protons as a second order effect. Nevertheless, with the set of differential Eqs. (22) and the boundary condition

<sup>7</sup>For  $N'_{A,i} = N_{A,i}/2$  for  $A = 2, 3, 4$  we redefine  $\Gamma_{A,i}^{\text{eff}} = 2\Gamma_{A,i}^{\text{eff}}$ .

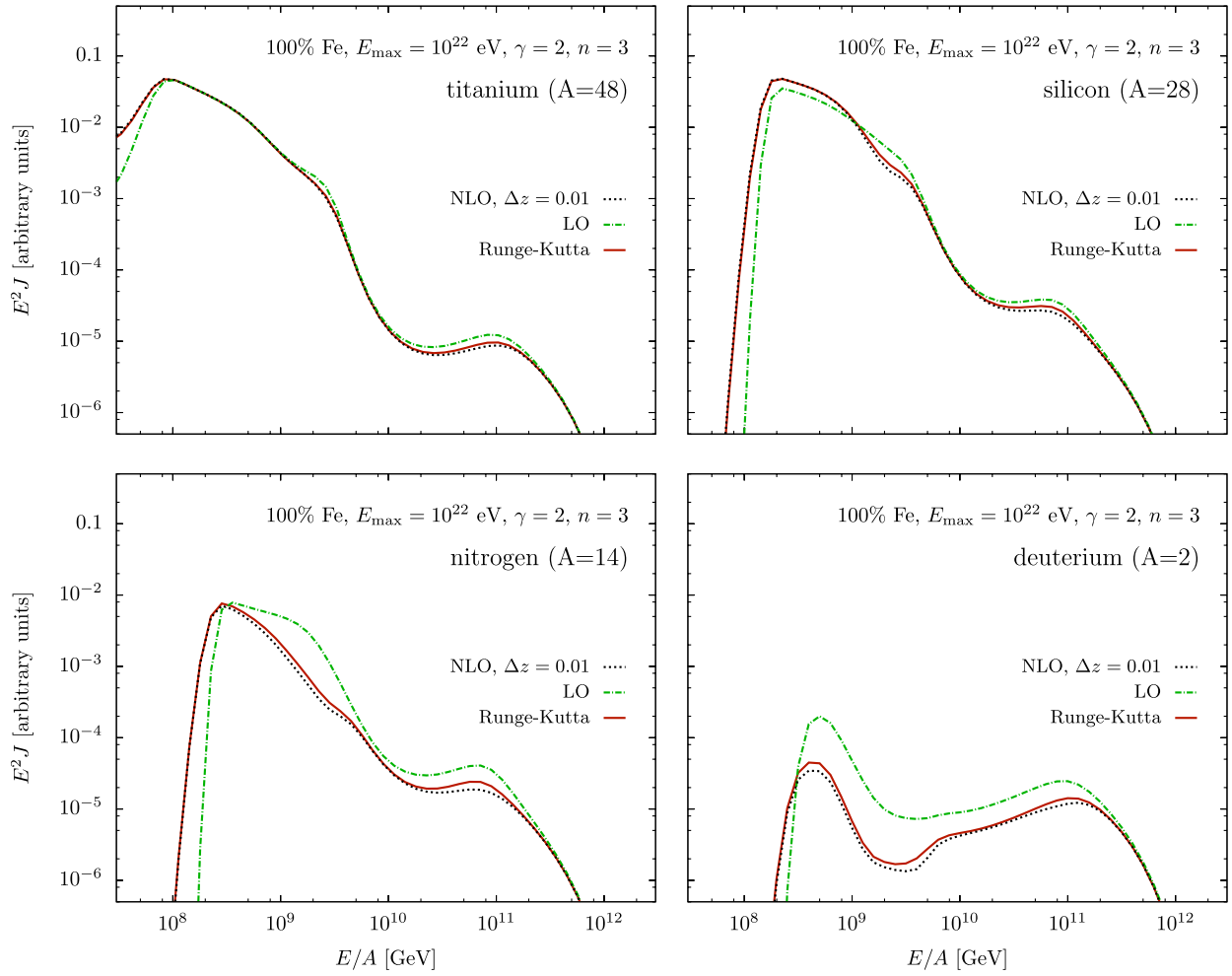


FIG. 6 (color online). The full NLO correction for two-nucleon and continuous energy losses in comparison with the numerical solution. For this result we took into account source evolution and redshift effects, assuming that the nucleon emission rates scale as  $(1+z)^3$  and sum over redshift steps  $\Delta z = 0.01$ .

$N_{1,i}^{(0)}(0) = N_{1,i}(0)$  and  $N_{1,i}^{(n)}(0) = 0$  for  $n > 0$  the expansion (9) is finite since the expansion of  $N_{A,i}$  is finite. Explicitly, we can write the  $n$ -th order contribution as

$$\begin{aligned}
 N_{1,i}^{(n)}(t) &= \sum_{B \geq 2} \sum_{j \geq i} \left( \prod_{k=i+1}^j \Gamma_{1,k}^{\text{CEL}} \right) \\
 &\times \sum_{k=i}^j \left[ \int_0^t dt' (\Gamma_{B,j}^{\text{eff}} N_{B,j}^{(n)}(t')) e^{-(t-t')\Gamma_{1,k}^{\text{CEL}}} \right] \\
 &\times \prod_{l=i(\neq k)}^j \frac{1}{\Gamma_{1,l}^{\text{CEL}} - \Gamma_{1,k}^{\text{CEL}}}. \quad (23)
 \end{aligned}$$

Again, these contributions to the proton spectra can be expressed via diagrams indicated in Fig. 7. By definition, the term  $N_{1,i}^{(n)}$  depend on all possible  $n$ -th order production chains of intermediate nuclei  $(B, j)$ , that are indicated as the boxes in the top right corner of the diagrams.

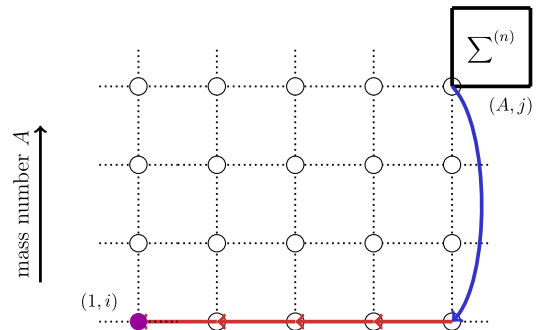


FIG. 7 (color online). An example of an  $n$ -th order production path contributing to  $N_{1,i}^{(n)}$  including the effective nucleon production rate  $\Gamma_{B,j}^{\text{eff}}$  (blue arrow). The box in the top right corners indicate the complete sum over all possible  $n$ -th order contributions “ $\sum^{(n)}$ ” to the production chain of the nucleus  $(B, j)$  with  $B \geq 2$  and  $j \geq i$ . The red arrows indicate the CEL contribution for protons, including energy loss by Bethe-Heitler pair production and photo-pion production.

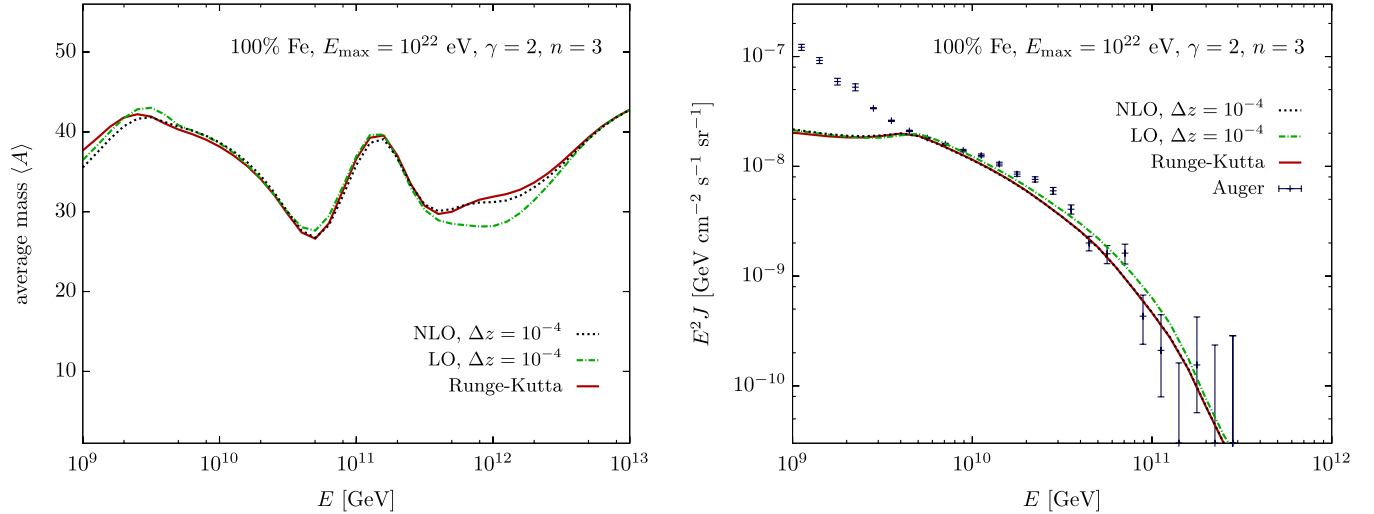


FIG. 8 (color online). *Left:* The average mass number from a pure-iron  $E^{-2}$  flux with  $E_{\max} = 10^{22}$  eV and source evolution parameters  $n = 3$  and  $z_{\max} = 1$ . We show the full numerical solution in comparison with the LO and NLO analytic equation including the exclusive channels  $(\gamma, N)$ ,  $(\gamma, 2N)$ ,  $(\gamma, \alpha)$ ,  $(\gamma, N\alpha)$  and  $(\gamma, 2\alpha)$  as well as CEL. *Right:* The total energy flux for the same parameters plotted against recent Auger measurements [2]. The LO results are in good agreement with those shown in Fig. 4 of [14].

Similarly, the emission of  $\alpha$  particles in the channels  $(\gamma, \alpha)$ ,  $(\gamma, 2\alpha)$  and  $(\gamma, N\alpha)$  rate can be described by the differential equation

$$\dot{N}_{4,i} \simeq \Gamma_{4,i+1}^{\text{CEL}} N_{4,i+1} - \Gamma_{4,i}^{\text{CEL}} N_{4,i} - (\Gamma_{4,i}^{\text{N}} + \Gamma_{4,i}^{\text{2N}}) N_{4,i} + \sum_{A \geq 2} \Gamma_{A,i}^{\text{eff},\alpha} N_{A,i} + \mathcal{Q}_{4,i}, \quad (24)$$

with an effective production rate

$$\Gamma_{A,i}^{\text{eff},\alpha} \equiv \Gamma_{A,i}^{\alpha} + \Gamma_{A,i}^{\text{N}\alpha} + 2\Gamma_{A,i}^{\text{2}\alpha} + \delta_{A12} \Gamma_{12,i}^{\text{2}\alpha} + \delta_{A9} \Gamma_{9,i}^{\text{N}\alpha} (+ \delta_{A8} \Gamma_{8,i}^{\alpha}). \quad (25)$$

Again, the last term in (25) is absent in the PSB chain considered in our calculation. In principle, we can treat these contributions analogously to the case of the protons. However, the relative contribution from  $\alpha$  particle emission is only small if we consider heavy primary nuclei like  $^{56}\text{Fe}$  and can be neglected in this case.

The sum over diagrams of the type shown in Fig. 7 involve a large number of intermediate configurations  $(B, j)$  and the calculation can become time-consuming. For a more efficient calculation of the proton spectra we can utilize the total conservation of nucleons per energy bin within sufficiently small time-steps with  $\Delta t \Gamma_{1,i}^{\text{CEL}} \ll 1$ . In this case the flux can be well approximated as

$$N_{1,i}(\Delta t) \simeq N_{1,i}(0) + \Delta t \mathcal{Q}_{1,i} + \Delta t [\Gamma_{1,i+1}^{\text{CEL}} N_{1,i+1}(0) - \Gamma_{1,i}^{\text{CEL}} N_{1,i}(0)] + \sum_{A \geq 2} A [N_{A,i}(0) + \Delta t \mathcal{Q}_{A,i} - N_{A,i}(\Delta t)]. \quad (26)$$

With this approximation, and using the NLO contribution of the exclusive channels  $(\gamma, N)$ ,  $(\gamma, 2N)$ ,  $(\gamma, \alpha)$ ,  $(\gamma, N\alpha)$

and  $(\gamma, 2\alpha)$  as well as CEL for the spectra of nuclei, we show in the left panel of Fig. 8 the average mass number  $\langle A \rangle$  in comparison with the analytic result. The right panel of Fig. 8 shows the total energy flux of nuclei for the NLO analytic solution compared to the numerical result. For these results, time steps of  $\Delta z = 10^{-4}$  have been used in order for the proton contribution to the total flux to be calculated with the necessary accuracy. The LO approximation is already in excellent approximation to the data of CR observatories considering the large systematic and statistical uncertainties of the CR spectra and the average mass composition. All spectral features of the quantities and their overall scale are well reproduced by the LO contribution. Improvements to the LO result, however, are made by the NLO contributions, whose results leave only a very mild discrepancy with the Runge-Kutta results at energies below  $10^{9.5}$  GeV.

## V. CONCLUSIONS

In this work we have developed further an analytic solution for the fluxes of UHE CR nuclei from extragalactic sources. We have shown that in most cases the spectra are well approximated by the analytic solution already given in Ref. [14], which dealt with the dominant energy loss channel of single nucleon transitions between nuclei. We have here expanded on this approach through the introduction of NLO corrections from two-nucleon and CEL. The introduction of these terms was shown to further improve the accuracy of the analytic description. In order for these results to take into account the slow variation of interaction and emission rates with redshift as well as CEL we incorporated our result into a semi-analytic framework. The semi-analytic results obtained were found to be in

excellent agreement with results obtained through a purely numerical Runge-Kutta approach.

The prospects of determining the nature of extragalactic UHE CRs and their sources in the near future are promising. Ongoing *direct* hybrid measurements of UHE CRs by the Auger collaboration continue, with the opportunity now existing for an independent verification of these results by other hybrid experiments such as the Telescope Array [32]. These measurements allow the possibility for a coherent picture of the UHE CR flux, composition, and arrival direction anisotropy to emerge. Present and ongoing *indirect* measurements of the secondary particles produced by UHE CRs during their acceleration and propagation are also capable of constraining the UHE CR composition and their sources. For instance, the simultaneous emission of neutrinos arising from proton-proton and/or proton-photon interactions in extragalactic protons sources can serve as a test of low energy crossover scenarios [8] of extragalactic protons [16,33]. Photo-pion interactions by extragalactic protons in the CMB, i.e. the process responsible for their Greisen-Zatsepin-Kuzmin cutoff, give rise to a flux of cosmogenic neutrinos [34–36] and photons [37]. The accompanying output into secondary electrons and positrons, in particular, from Bethe-Heitler pair production, feeds into electromagnetic cascades in the cosmic background radiation and intergalactic magnetic fields [38]. This leads to the accumulation of  $\gamma$  rays at GeV-TeV energies. The observed extragalactic diffuse  $\gamma$ -ray flux thus provides a constraint on the total energy injected into such cascades over the Universe’s entire history [39].

The methods provided in this paper offer a general tool with which theoretical results may be easily obtained and compared to both these *direct* and *indirect* UHE CR measurements. As example cases, the application of the general methods developed here to proton propagation provide the opportunity to further develop the method applied in [40]. Second, an analytic determination of the photon fraction produced through UHE CR nuclei propagation is anticipated to also be obtainable using this treatment. Through the simplicity of our approach, the speed with which it may be implemented, and the intuitive understanding it introduces, our analytic method is anticipated to be of great benefit as a tool for future UHE CR investigations.

### ACKNOWLEDGMENTS

We thank J. Salvadó for his help on a numerical evaluation of the cosmic ray spectra via a Runge-Kutta method. M. A. acknowledges support by the Research Foundation of SUNY at Stony Brook.

### APPENDIX A: PHOTO-DISINTEGRATION OF NUCLEI

The most general evolution of primary and secondary nuclei in the CRB includes all possible photo-

disintegration transitions between nuclides  $(A, Z)$  competing with the decay of unstable nuclides. For simplicity, we follow the work of PSB [17–19] and consider only one stable isotope per mass number  $A$  in the decay chain of  $^{56}\text{Fe}$  as already explained in section II. This “PSB chain” is listed in Table I and sketched in Fig. 9.

Table I shows the relative contribution of inclusive channels to the total photo-disintegration rate calculated for the nuclei of the PSB chain. We use the reaction code TALYS [20] to evaluate the cross sections for nuclei with  $10 \leq A \leq 56$  and assume an  $E^{-2}$  power-law flux of CR nuclei. At CR energies  $E < 10^{12}$  GeV and large mass numbers  $A \geq 20$  photo-disintegration in the CRB can be well approximated by one-nucleon and two-nucleon losses between elements of the PSB chain via exclusive processes  $(\gamma, p)$ ,  $(\gamma, n)$ ,  $(\gamma, 2p)$ ,  $(\gamma, 2n)$  and  $(\gamma, pn)$ . For the cross sections of light nuclei with mass numbers  $A = 2, 3, 4$  and 9 we use the parameterization of Ref. [41].

At lower mass numbers,  $A \leq 20$ , additional channels involving  $\alpha$  particle emission can become as significant as the sum of one-nucleon and two-nucleon losses. Table I also shows the relative importance of the exclusive channels  $(\gamma, \alpha)$ ,  $(\gamma, n\alpha)$ ,  $(\gamma, p\alpha)$  and  $(\gamma, 2\alpha)$  to the total photo-disintegration budget. Resonant photo-nuclear interactions play only a minor role in the propagation of the nuclei for the energies of interest. We follow the approach outlined in Ref. [41] and approximate the total interaction by the isospin averaged  $N\gamma$  rate as  $\Gamma_{A\gamma}(z, E) \simeq A\Gamma_{N\gamma}(z, E/A)$ . We also assume that the participating nucleon is removed from the nucleus and regard this as a contribution to one-nucleon losses.

The angle-averaged interaction rate appearing in Eq. (1) is then defined as

$$\Gamma_{A \rightarrow B}(z, E) = \frac{1}{2} \int_{-1}^1 d \cos \theta \int d\epsilon (1 - \beta \cos \theta) n_{\gamma}(z, \epsilon) \sigma_{A \rightarrow B}(\epsilon'), \quad (\text{A1})$$

where  $n_{\gamma}(z, \epsilon)$  is the energy distribution of isotropic background photons at redshift  $z$  and  $\epsilon' = \epsilon\gamma(1 - \beta \cos \theta)$  the photon’s energy in the rest frame of the nucleus. For our calculation we use the cosmic microwave background and the infrared/optical background from Ref. [22]. To a good approximation the decay products of the photo-disintegration interaction inherit the large boost factor of the initial nucleus and hence in the process  $A \rightarrow B + (A - B)$  the nucleus with mass number  $B$  has an energy  $E' = (B/A)E$ . We can hence approximate the differential cross section as

$$\gamma_{A \rightarrow B}(E, E') \simeq \Gamma_{A \rightarrow B}(E) \delta((B/A)E - E') \quad (\text{A2})$$

in the following. This has the correct normalization since  $\Gamma_{A \rightarrow B}(E) \equiv \int dE' \gamma_{A \rightarrow B}(E, E')$ .

In general, the interaction rates  $\Gamma_{A \rightarrow B}(z, E)$  scale with redshift according to the redshift evolution of the radiation

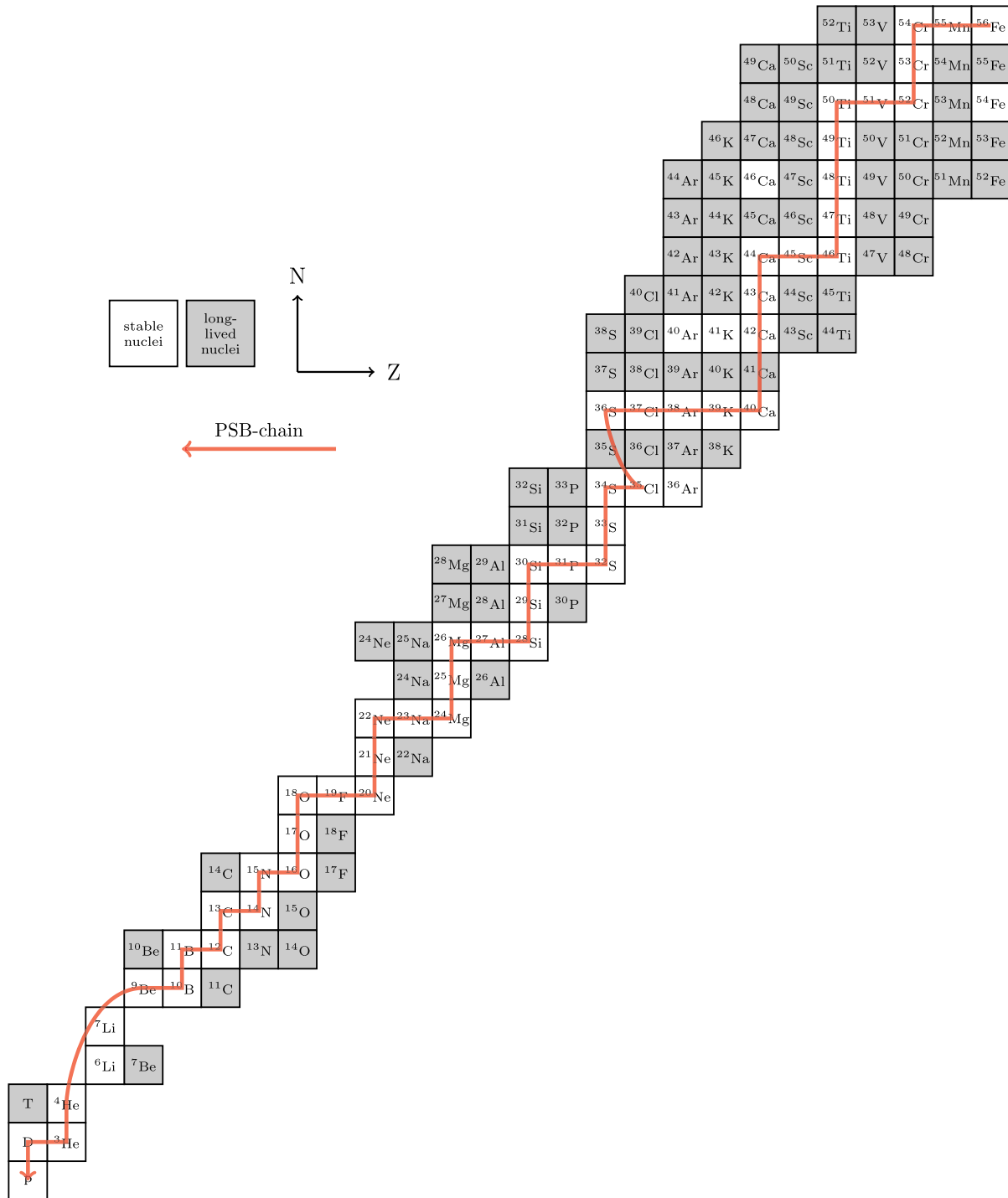


FIG. 9 (color online). The *Puget-Stecker-Bredekamp* chain [18] along with stable and long-lived ( $\tau \geq 1$  min) nuclei below  $^{56}\text{Fe}$ .

background. In the case of the CMB with adiabatically scaling,  $n_\gamma(z, \epsilon) = (1+z)^2 n_\gamma(0, \epsilon/(1+z))$ , we can derive the simple relation

$$\Gamma_{A \rightarrow B}(z, E_i) = (1+z)^3 \Gamma_{A \rightarrow B}(0, (1+z)E). \quad (\text{A3})$$

For the case of the infrared/optical background [22] we assume a redshift scaling following the star formation rate

as described in Ref. [16]. However, since the cascades of UHE CR nuclei develop locally, the redshift dependence of the interaction rates is only of minor importance.

## APPENDIX B: PROOF OF EQUATION (4)

We will proof Eq. (4) by induction. First note, that we can rewrite Eq. (4) as

$$\dot{N}_i = -\Gamma_i^{\text{tot}} N_i + \sum_{j=i+1}^n \Gamma_{j \rightarrow i} N_j + Q_i, \quad (\text{B1})$$

with  $i = 1, \dots, n$  with  $\Gamma_{j \rightarrow i} = 0$  for  $i \leq j$  and  $\Gamma_i^{\text{tot}} \neq \Gamma_j^{\text{tot}}$  for  $i \neq j$ . In the following we will refer to the indices  $i$  as *knots* and the pairs  $(i, j)$  with  $\Gamma_{i \rightarrow j} \neq 0$  as *links*. A *chain* of length  $n_c$  is defined as an ascending sequence of  $n_c$  knots,  $c_1 < c_2 < \dots < c_{n_c}$ , that are mutually connected by links.

We want to show that the most general solution of Eq. (B1) is of the form

$$N_i(t) = \sum_{j \leq i} \sum_{\mathbf{c}} \left( \prod_{l=1}^{n_c-1} \Gamma_{c_l \rightarrow c_{l+1}} \right) \sum_{k=1}^{n_c} \left[ N_j(0) e^{-t \Gamma_{c_k}^{\text{tot}}} + \int_0^t dt' Q_j(t') e^{-(t-t') \Gamma_{c_k}^{\text{tot}}} \right] \prod_{p=1(\neq k)}^{n_c} \frac{1}{\Gamma_{c_p}^{\text{tot}} - \Gamma_{c_k}^{\text{tot}}} \quad (\text{B2})$$

where the sum is over all possible chains  $\mathbf{c}$  with  $c_1 = j$  and  $c_{n_c} = i$ .

*Induction start:*  $n = 1$ . This case has the solution

$$N_1(t) = N_1(0) e^{-t \Gamma_1^{\text{tot}}} + \int_0^t dt' Q_1(t') e^{-(t-t') \Gamma_1^{\text{tot}}}.$$

This is of the form (B2), since the only chain is the trivial one of length  $n_c = 1$  with  $c_1 = 1$ .

*Induction step:*  $n \rightarrow n + 1$ . The differential equations of  $N_i$  with  $1 \leq i \leq n$  are of the form (B1) and we can hence use the solution (B2). The differential equation for  $N_{n+1}$  is

$$\dot{N}_{n+1} = -\Gamma_{n+1}^{\text{tot}} N_{n+1} + \sum_{m=1}^n \Gamma_{m \rightarrow n+1} N_m + Q_{n+1}. \quad (\text{B3})$$

We can write the general solution of this differential equation as

$$N_{n+1}(t) = \left[ N_{n+1}(0) e^{-t \Gamma_{n+1}^{\text{tot}}} + \int_0^t dt' Q_{n+1}(t') e^{-(t-t') \Gamma_{n+1}^{\text{tot}}} \right] + \int_0^t dt' e^{-(t-t') \Gamma_{n+1}^{\text{tot}}} \sum_{m=1}^n \Gamma_{m \rightarrow n+1} N_m(t'). \quad (\text{B4})$$

The first term of the previous equation corresponds to the first term ( $i = j = n + 1$ ) in the sum of Eq. (B2). Inserting the solutions (B2) in the integrand yields after integration by parts:

$$N_{n+1}(t) = \left[ N_{n+1}(0) e^{-t \Gamma_{n+1}^{\text{tot}}} + \int_0^t dt' Q_{n+1}(t') e^{-(t-t') \Gamma_{n+1}^{\text{tot}}} \right] + \sum_{m=1}^n \sum_{j=1}^m \sum_{\mathbf{c}} \left( \prod_{l=1}^{n_c-1} \Gamma_{c_l \rightarrow c_{l+1}} \right) \Gamma_{m \rightarrow n+1} \sum_{k=1}^{n_c} \left( \prod_{p=1(\neq k)}^{n_c} \frac{1}{\Gamma_{c_p}^{\text{tot}} - \Gamma_{c_k}^{\text{tot}}} \right) \times \frac{1}{\Gamma_{n+1}^{\text{tot}} - \Gamma_{c_k}^{\text{tot}}} \left( \left[ N_j(0) e^{-t \Gamma_{c_k}^{\text{tot}}} + \int_0^t dt' Q_j(t') e^{-(t-t') \Gamma_{c_k}^{\text{tot}}} \right] - \left[ N_j(0) e^{-t \Gamma_{n+1}^{\text{tot}}} + \int_0^t dt' Q_j(t') e^{-(t-t') \Gamma_{n+1}^{\text{tot}}} \right] \right). \quad (\text{B5})$$

The chains  $\mathbf{c}$  in the previous sums have end-points  $c_1 = j$  and  $c_{n_c} = m$ . Now, every chain  $\mathbf{c}$  in the system with  $n$  knots and endpoint  $c_{n_c} = m$  corresponds *unambiguously* to a chain  $\mathbf{c}'$  in the system with  $n + 1$  knots with  $c'_i = c_i$  for  $i \leq n_c - 1$  and  $c'_{n_c} = n + 1$ . Hence, the double sum in Eq. (B5) over end points  $m < n$  and chains  $\mathbf{c}$  can be expressed as a single sum over chains  $\mathbf{c}'$  with  $c'_1 = j$  and  $c'_{n_c} = n + 1$ . We arrive at the form:

$$N_{n+1}(t) = \left[ N_{n+1}(0) e^{-t \Gamma_{n+1}^{\text{tot}}} + \int_0^t dt' Q_{n+1}(t') e^{-(t-t') \Gamma_{n+1}^{\text{tot}}} \right] + \sum_{j=1}^n \sum_{\mathbf{c}'} \left( \prod_{l=1}^{n_c'-1} \Gamma_{c'_l \rightarrow c'_{l+1}} \right) \sum_{k=1}^{n_c'-1} \left[ N_j(0) e^{-t \Gamma_{c'_k}^{\text{tot}}} + \int_0^t dt' Q_j(t') e^{-(t-t') \Gamma_{c'_k}^{\text{tot}}} \right] \prod_{p=1(\neq k)}^{n_c'} \frac{1}{\Gamma_{c'_p}^{\text{tot}} - \Gamma_{c'_k}^{\text{tot}}} - \sum_{j=1}^n \sum_{\mathbf{c}'} \left( \prod_{l=1}^{n_c'-1} \Gamma_{c'_l \rightarrow c'_{l+1}} \right) \left[ N_j(0) e^{-t \Gamma_{n+1}^{\text{tot}}} + \int_0^t dt' Q_j(t') e^{-(t-t') \Gamma_{n+1}^{\text{tot}}} \right] \sum_{k=1}^{n_c'-1} \prod_{p=1(\neq k)}^{n_c'} \frac{1}{\Gamma_{c'_p}^{\text{tot}} - \Gamma_{c'_k}^{\text{tot}}}. \quad (\text{B6})$$

As a final step we use the identity<sup>8</sup>:

$$\sum_{k=1}^{n_c'-1} \prod_{p=1(\neq k)}^{n_c'} \frac{1}{\Gamma_{c'_p}^{\text{tot}} - \Gamma_{c'_k}^{\text{tot}}} = - \prod_{p=1}^{n_c'-1} \frac{1}{\Gamma_{c'_p}^{\text{tot}} - \Gamma_{n+1}^{\text{tot}}}, \quad (\text{B7})$$

to combine the last two terms in Eq. (B6) and arrive at the form (B2).

<sup>8</sup>See the appendix of Ref. [14] for a simple derivation of this expression.

- [1] M. Nagano and A. A. Watson, *Rev. Mod. Phys.* **72**, 689 (2000).
- [2] J. Abraham *et al.* (Pierre Auger Collaboration), *Phys. Lett. B* **685**, 239 (2010).
- [3] J. Abraham *et al.* (Pierre Auger Collaboration), *Phys. Rev. Lett.* **104**, 091101 (2010).
- [4] R. Abbasi *et al.* (HiRes Collaboration), *Phys. Rev. Lett.* **100**, 101101 (2008).
- [5] R. U. Abbasi *et al.* (HiRes Collaboration), *Phys. Rev. Lett.* **104**, 161101 (2010).
- [6] J. Linsley, in *Proceedings of ICRC 1963, Jaipur, India*, (Commercial Printing Press, Ltd., Bombay, India, 1964) p. 77.
- [7] C. T. Hill and D. N. Schramm, *Phys. Rev. D* **31**, 564 (1985).
- [8] V. Berezhinsky, A. Z. Gazizov, and S. I. Grigorieva, *Phys. Rev. D* **74**, 043005 (2006).
- [9] Z. Fodor, S. D. Katz, A. Ringwald, and H. Tu, *J. Cosmol. Astropart. Phys.* **11** (2003) 015.
- [10] K. Greisen, *Phys. Rev. Lett.* **16**, 748 (1966).
- [11] G. T. Zatsepin and V. A. Kuzmin, *Pis'ma Zh. Eksp. Teor. Fiz.* **4**, 114 (1966) [*JETP Lett.* **4**, 78 (1966)].
- [12] J. Abraham *et al.* (Pierre Auger Collaboration), *Phys. Rev. Lett.* **101**, 061101 (2008).
- [13] C. AMSLER *et al.* (Particle Data Group), *Phys. Lett. B* **667**, 1 (2008).
- [14] D. Hooper, S. Sarkar, and A. M. Taylor, *Phys. Rev. D* **77**, 103007 (2008).
- [15] R. Aloisio, V. Berezhinsky, and S. Grigorieva, [arXiv:0802.4452](https://arxiv.org/abs/0802.4452); [arXiv:1006.2484](https://arxiv.org/abs/1006.2484).
- [16] M. Ahlers, L. A. Anchordoqui, and S. Sarkar, *Phys. Rev. D* **79**, 083009 (2009).
- [17] F. W. Stecker, *Phys. Rev.* **180**, 1264 (1969).
- [18] J. L. Puget, F. W. Stecker, and J. H. Bredekamp, *Astrophys. J.* **205**, 638 (1976).
- [19] F. W. Stecker and M. H. Salamon, *Astrophys. J.* **512**, 521 (1999).
- [20] S. Goriely, S. Hilaire, and A. J. Koning, *Astron. Astrophys.* **487**, 767 (2008), <http://www.talys.eu/>.
- [21] G. R. Blumenthal, *Phys. Rev. D* **1**, 1596 (1970).
- [22] A. Franceschini, G. Rodighiero, and M. Vaccari, *Astron. Astrophys.* **487**, 837 (2008).
- [23] P. P. Kronberg, *Rep. Prog. Phys.* **57**, 325 (1994).
- [24] A. Neronov and I. Vovk, *Science* **328**, 73 (2010).
- [25] K. Dolag, D. Grasso, V. Springel, and I. Tkachev, *J. Cosmol. Astropart. Phys.* **01** (2005) 009.
- [26] R. Aloisio and V. Berezhinsky, *Astrophys. J.* **612**, 900 (2004).
- [27] R. Aloisio and V. S. Berezhinsky, *Astrophys. J.* **625**, 249 (2005).
- [28] GNU Multiple Precision Arithmetic Library 5.0.1, <http://gmplib.org/>.
- [29] GNU Multiple Precision Floating-Point Reliable Library 3.0.0, <http://www.mpfr.org/>.
- [30] GNU Scientific Library 1.14, <http://www.gnu.org/software/gsl/>.
- [31] A. Mücke, R. Engel, J. P. Rachen, R. J. Protheroe, and T. Stanev, *Comput. Phys. Commun.* **124**, 290 (2000).
- [32] H. Tokuno *et al.*, *AIP Conf. Proc.* **1238**, 365 (2010).
- [33] M. Ahlers, L. A. Anchordoqui, H. Goldberg, F. Halzen, A. Ringwald, and T. J. Weiler, *Phys. Rev. D* **72**, 023001 (2005).
- [34] F. W. Stecker, *Astrophys. J.* **228**, 919 (1979).
- [35] S. Yoshida and M. Teshima, *Prog. Theor. Phys.* **89**, 833 (1993); R. J. Protheroe and P. A. Johnson, *Astropart. Phys.* **4**, 253 (1996); R. Engel, D. Seckel, and T. Stanev, *Phys. Rev. D* **64**, 093010 (2001).
- [36] D. Hooper, A. Taylor, and S. Sarkar, *Astropart. Phys.* **23**, 11 (2005); M. Ave, N. Busca, A. V. Olinto, A. A. Watson, and T. Yamamoto, *Astropart. Phys.* **23**, 19 (2005); D. Allard *et al.*, *J. Cosmol. Astropart. Phys.* **09** (2006) 005; L. A. Anchordoqui, H. Goldberg, D. Hooper, S. Sarkar, and A. M. Taylor, *Phys. Rev. D* **76**, 123008 (2007); K. Kotera, D. Allard, and A. V. Olinto, *J. Cosmol. Astropart. Phys.* **10** (2010) 013.
- [37] D. Hooper, A. M. Taylor, and S. Sarkar, [arXiv:1007.1306](https://arxiv.org/abs/1007.1306).
- [38] R. J. Protheroe and T. Stanev, *Mon. Not. R. Astron. Soc.* **264**, 191 (1993); S. Lee, *Phys. Rev. D* **58**, 043004 (1998).
- [39] For recent evaluations see, V. Berezhinsky, A. Gazizov, M. Kachelriess, and S. Ostapchenko, [arXiv:1003.1496](https://arxiv.org/abs/1003.1496); M. Ahlers, L. A. Anchordoqui, M. C. Gonzalez-Garcia, F. Halzen, and S. Sarkar, *Astropart. Phys.* **34**, 106 (2010).
- [40] A. M. Taylor and F. A. Aharonian, *Phys. Rev. D* **79**, 083010 (2009).
- [41] J. P. Rachen, Ph.D. thesis Bonn University, 1996.